



Technical Note

Absolute Radiometric Calibration of ZY3-02 Satellite Multispectral Imager Based on Irradiance-Based Method

Hongzhao Tang¹, Junfeng Xie^{1,*}, Wei Chen² , Honggeng Zhang^{1,2} and Hengyang Wang³¹ Land Satellite Remote Sensing Application Center, Ministry of Natural Resources, Beijing 100094, China² College of Geoscience and Surveying Engineering, China University of Mining and Technology, Beijing 100083, China³ Changchun Institute of Optics, Fine Mechanics and Physics, University of Chinese Academy of Sciences, Changchun 130033, China

* Correspondence: xiejf@lasac.cn; Tel.: +86-10-6841-2293

Abstract: In this paper, an irradiance-based absolute radiometric calibration campaign at Baotou calibration site during June and July 2018 was described. This radiometric calibration campaign made use of six radiometric calibration tarps. The synchronous measurements of parameters such as surface reflectance, atmospheric parameters, and diffuse-to-global irradiance ratio were collected at the satellite overpass. The top-of-atmospheric radiance was predicted by radiative transfer model with these synchronous measurements. The linear relationship between DN of satellite sensor and band-specific top-of-atmospheric spectral radiance was established, and a stable and reliable absolute calibration coefficient of ZY3-02 MUX was determined in this campaign. We compared the calibration results of the irradiance-based method with those of the reflectance-based method. The results suggested that the irradiance-based method is better than reflectance-based method.

Keywords: ZY3-02; radiometric calibration; irradiance-based method; absolute radiation calibration method of irradiance-based



Citation: Tang, H.; Xie, J.; Chen, W.; Zhang, H.; Wang, H. Absolute Radiometric Calibration of ZY3-02 Satellite Multispectral Imager Based on Irradiance-Based Method. *Remote Sens.* **2023**, *15*, 448. <https://doi.org/10.3390/rs15020448>

Academic Editor: Lunche Wang

Received: 7 December 2022

Revised: 8 January 2023

Accepted: 9 January 2023

Published: 11 January 2023



Copyright: © 2023 by the authors. Licensee MDPI, Basel, Switzerland. This article is an open access article distributed under the terms and conditions of the Creative Commons Attribution (CC BY) license (<https://creativecommons.org/licenses/by/4.0/>).

1. Introduction

To obtain extremely precise Earth surface measurements, the absolute radiometric calibration of optical satellites is a crucial process. [1]. Absolute radiometric calibration establishes the link between the imaging DN value and the sensor's top-of-atmospheric radiance. [2]. The reflectance-based approach, the irradiance-based method, and the radiance-based method are the three main on-orbit absolute radiometric calibration techniques. [3]. The reflectance-based method proposed by Slater in University of Arizona has become the most commonly used method for in-flight absolute radiometric calibration of satellites sensor [4]. This method had been widely used for calibration by various satellite sensors, such as IKONOS and SPOT satellite sensors, as well as China's FengYun series [5–10].

On 30 May 2016, ZY3-02 satellite continued the Chinese civil high-resolution stereoscopic mapping satellite system. ZY3-02 satellite is loaded with four optical cameras: one multispectral imager sensor (MUX) and three cameras with panchromatic wavelength ranges (TLC). This satellite played an important role in quantitative remote sensing applications for China's industry applications. To maintain the high-accuracy radiometric characteristic of ZY3-02 satellite, a vicarious calibration campaign was conducted by Land Satellite Remote Sensing Application Center (LASAC) each year [11,12]. A reliable radiometric calibration coefficient was obtained by the reflectance-based absolute radiometric calibration method in these campaigns, especially for the ZY3-02 satellite sensors.

However, the aerosol model in the radiative transfer model assumes the maximum error that may occur in the absolute refractive index calibration method as the reflectivity. The larger the aerosol optical depth (AOD), the larger the contribution in radiative transfer simulations, and the aerosol model is particularly sensitive for calculating the at-sensor

(top-of-atmospheric, TOA) radiance by the radiative transfer model. The assumption of the aerosol model in the radiative transfer model will bring large errors to the reflectance-based absolute radiometric calibration. The irradiance-based approach is utilized in this study to reduce the overall uncertainty that is contributed by the assumption of aerosol model parameters in the radiative transfer model while using reflectance-based method.

This study describes an enhanced calibration campaign based on the irradiance-based approach. For radiometric calibration, a collection of several tarpaulins was created. In this campaign, synchronized measurements of aerosol optical depth (AOD) and surface reflectance were taken at the satellite flyover. Using an AG-512 SSIR Solar Spectroradiometer, the ratio of diffuse-to-global downward irradiance at the surface level was determined. Based on these synchronous data and the ratio of diffuse radiation to global downward irradiance, the top of atmosphere (TOA) radiation is predicted. In the ZY3-02 MUX images, the connection between Digital Number (DN) value and TOA radiation was found, and the radiometric calibration coefficients were calculated. In this research, the calibration outcomes of the reflectance-based approach and the irradiance-based method were compared.

2. Materials and Methods

2.1. ZY3-02 Satellite Background

The ZY3-02 satellite enters 505 km sun-synchronous orbit, and it made one complete round of the world every 59 days [12]. ZY3-02 satellite carried four optical cameras: three panchromatic cameras and a multispectral imager. The details of ZY3-02 satellite and MUX [12] are shown in Table 1. Figure 1 shows the normalized spectral response function (SRF) of ZY3-02 MUX.

Table 1. Details of ZY3-02 satellite.

ZY3-02 Satellite	Detailed Information
Spectral Bands	Panchromatic band: 0.45–0.9 μm Blue band: 0.45–0.52 μm Green band: 0.52–0.59 μm Red band: 0.63–0.69 μm NIR band: 0.77–0.89 μm
Spatial resolution	Panchromatic band: nadir-view: 2.1 m (GSD) forward-view (+22°): 2.5 m (GSD) backward-view (−22°): 2.5 m (GSD) Multispectral: nadir-view: 5.8 m (GSD)
Radiometric Resolution	10 bits
Swath width	51 km

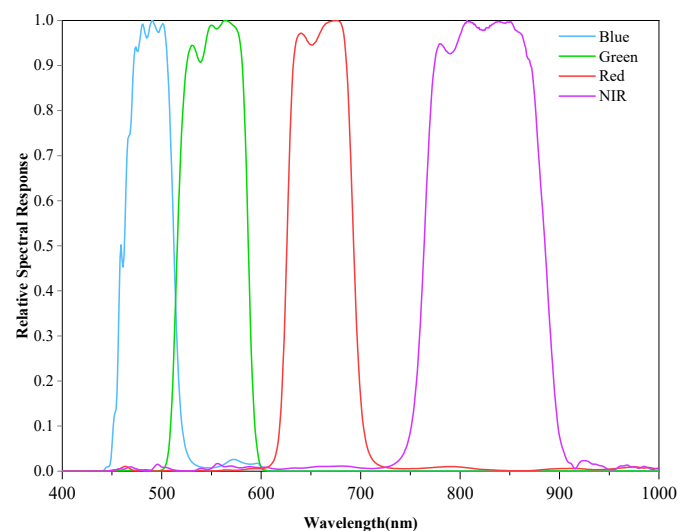


Figure 1. Details of normalized spectral response function of multispectral sensor (MUX).

2.2. Irradiance-Based Absolute Radiometric Calibration Method

This paper proposes an absolute radiometric calibration method for irradiance. The flow of infrared radiation based technology is shown in Figure 2.

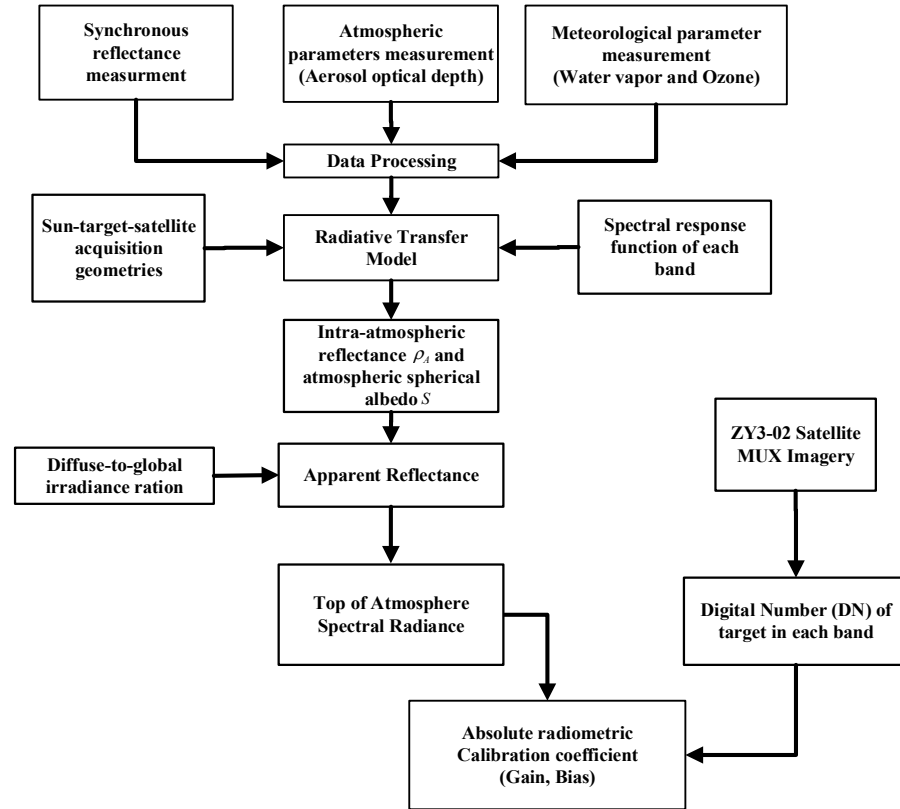


Figure 2. Technical process of on-orbit absolute radiometric calibration of multispectral sensor (MUX) based on irradiance-based method.

The irradiance-based absolute radiometric calibration method, the same as the reflectance-based method, mainly relies on synchronous atmospheric parameters and the surface's reflectance measurements. The ratio of diffuse-to-global downward irradiance at the ground level was measured to improve the reflectance-based method.

The apparent reflectance of the ZY3-02 satellite MUX $\rho^*(\theta_s, \theta_v, \varphi_v - \varphi_s)$ can be expressed as:

$$\rho^*(\theta_s, \theta_v, \Delta\varphi) = T_g(\mu_s, \mu_v) \left[\rho_A(\theta_s, \theta_v, \Delta\varphi) + \frac{\tau(\mu_s) \cdot \rho \cdot \tau(\mu_v)}{1 - \rho \cdot S} \right] \quad (1)$$

where θ_s is the solar zenith angle, φ_s is the solar azimuth angle, θ_v is the viewing zenith angle, φ_v is the viewing azimuth angle, and $\Delta\varphi$ is the relative azimuth angle. $\rho_A(\theta_s, \theta_v, \Delta\varphi)$ is the path reflectance contributed by atmosphere, S is defined as atmospheric spherical albedo, $T_g(\mu_s, \mu_v)$ is the gaseous transmittance, $\tau(\mu_s)$ is total transmittance from the solar to the object, and $\tau(\mu_v)$ is the total transmittance from the object to the sensor.

$\tau(\mu_s)$ can be expressed as:

$$\tau(\mu_s) = e^{-\frac{\delta}{\mu_s}} + \frac{\int_0^{2\pi} \int_0^1 L^0(\mu, \mu_s, \Delta\varphi) \mu d\mu d\varphi}{\mu_s E_s} = e^{-\frac{\delta}{\mu_s}} + \frac{E_d^0}{\mu_s E_s} \quad (2)$$

where L^0 and E_d^0 are the downward radiance and irradiance at the surface level by atmospheric scattering, δ is the atmospheric optical depth, and E_s is the solar irradiance at the TOA.

The diffuse-to-global ratio from the solar to the object α_s is defined as:

$$\alpha_s = \frac{E_d(\mu_s)}{E_G(\mu_s)} = \frac{E_d(\mu_s)}{\mu_s \cdot E_s \cdot e^{-\frac{\delta}{\mu_s}} + E_d(\mu_s)} \quad (3)$$

where $E_G(\mu_s)$ is the global irradiance, $E_d(\mu_s)$ is the diffuse irradiance, and $\mu_s E_s \frac{\tau(\mu_v)}{1-\rho \cdot S}$ is the direct solar irradiance.

$E_d(\mu_s)$ is defined as:

$$E_d(\mu_s) = \frac{1}{1-\rho \cdot S} \left[E_d^0(\mu_s) + \mu_s E_s e^{-\frac{\delta}{\mu_s}} \cdot \rho \cdot S \right] \quad (4)$$

The total transmittance from the solar to the earth $\tau(\mu_s)$ can be expressed as:

$$\tau(\mu_s) = \frac{(1-\rho \cdot S) e^{-\frac{\delta}{\mu_s}}}{1-\alpha_s} \quad (5)$$

According to the reciprocity principle, the total transmittance from the object to the satellite sensor $\tau(\mu_v)$ can be expressed as:

$$\tau(\mu_v) = \frac{(1-\rho \cdot S) e^{-\frac{\delta}{\mu_v}}}{1-\alpha_v} \quad (6)$$

Now $\rho^*(\theta_s, \theta_v, \Delta\varphi)$ can be expressed as:

$$\rho^*(\theta_s, \theta_v, \Delta\varphi) = T_g(\mu_s, \mu_v) \left[\rho_A(\theta_s, \theta_v, \Delta\varphi) + \frac{e^{-\frac{\delta}{\mu_s}}}{1-\alpha_s} \rho (1-\rho \cdot S) \cdot \frac{e^{-\frac{\delta}{\mu_v}}}{1-\alpha_v} \right] \quad (7)$$

The TOA radiance $L(\theta_s, \theta_v, \Delta\varphi)$ can be expressed with apparent reflectance $\rho^*(\theta_s, \theta_v, \Delta\varphi)$:

$$L(\theta_s, \theta_v, \Delta\varphi) = \frac{\mu_s E_s \rho^*(\theta_s, \theta_v, \Delta\varphi)}{\pi d^2} \quad (8)$$

where E_s is the solar irradiance at TOA; $\mu_s = \cos\theta_s$, d is the earth-sun distance in astronomical units.

Calculate the relationship between TOA spectral radiation and target DN based on Equation (9):

$$L = Gain * DN + Bias \quad (9)$$

where L is the TOA radiance, DN is the digital number got from MUX images, and $Gain$ and $Bias$ are the radiometric calibration coefficients.

2.3. The Vicarious Radiometric Calibration Campaign

An improved calibration campaign using the irradiance-based method was performed between June and July 2018 at Baotou calibration site on two separate days: 28 June, 3 July, 2018. Table 2 displays the solar-target-satellite acquisition geometric circumstances of ZY3-02 satellite at Baotou Site. For this radiometric calibration endeavor, many radiometric calibration tarps were created. At the satellite overpass, reflectance of the radiometric calibration tarps, AOD, and the ratio of diffuse-to-global downwards irradiance at surface level was observed.

Table 2. Geometric conditions of the three ZY3-02 overpasses at Baotou calibration site in 2018.

Site	Date	Satellite Overpass Time (UTC)	Solar Zenith Angle	Solar Azimuth Angle	Viewing Zenith Angle	Viewing Azimuth Angle
Baotou calibration site	28 June 2018	03:35:22	20.497	146.015	5.872	208.995
	3 July 2018	03:39:18	21.573	145.360	−1.394	151.594

Baotou calibration site is located 40.8°N and 109.6°E at about 1300 m above sea level. Located in Inner Mongolia Province, China, and the flat area of the Baotou calibration location is around 360 km². [13]. This location is on flat terrain in a semiarid zone where bare soil and sand predominate. [14]. A set of four gray-scale radio-metric calibration tarps with nominal reflectance of 5%, 20%, 40%, and 60%, as well as two color-scaled tarps (red and blue), were created and placed at this calibration site to be able to correctly calibrate the ZY3-02 Satellite MUX. An ideal calibration tarp should be physically robust over time, reasonably level, and homogeneous in spectrum terms, with little to no fluctuation in the surface feature. [15]. For on-orbit absolute radiometric calibration, these radiometric calibration tarps were built with quasi-Lambertian characteristics. Each calibration tarp is 3600 m² in size, and the spatial variance of each radiometric calibration tarp is strictly limited to less than 2%. Figure 3 depicts the bi-directional reflectance factor (BRF) measured in laboratory of the 5%, 20%, 40%, and 60% calibration tarps. The spectral variance in reflectance of these four tarps is less than 3%. [12]. The placement of the radiometric calibration tarps is seen in Figure 4.

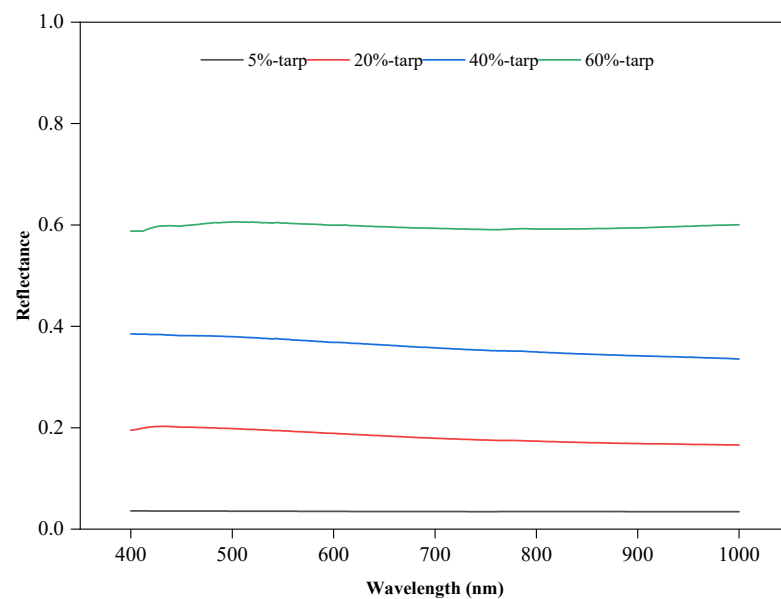
**Figure 3.** The laboratory measured BRF of the calibration tarps.



Figure 4. The spatial layout of the radiometric calibration tarps in this study at Baotou site.

2.4. Synchronous Reflectance and Atmospheric Parameters Measurements

The four gray-scale and two color radiometric calibration tarps were 3600 m², covering about 10 × 10 pixels in the MUX image. Each single tarp in this study was divided into 5 × 5 samples, and 25 samples were collected within 10 min by spectroradiometer. The SVC HR-1024i spectroradiometer (spectral range of 350–2500 nm) collected the reflectance. Within 30 min of the satellite flyover time, the surface reflectance measurement was completed. It is noteworthy that five spectra were collected in each sample of each single tarp; 750 spectra of the calibration tarps were collected in every calibration campaign.

A CIMEL CE318 sun photometer was used to detect the total columnar water vapor (CWV) and aerosol optical depth (AOD) once every 3 min during the calibration campaign. Table 3 and Figure 5 show the measurement of AOD and CWV at Baotou site on 28 June 2018.

Table 3. Synchronous atmospheric parameters measurements.

Atmospheric Parameters Measured	Measurement Results	
Date	28 June 2018	3 July 2018
AOD @ 550 nm	0.2655	0.0760
CWV	1.2351 g/cm ²	0.8132 g/cm ²

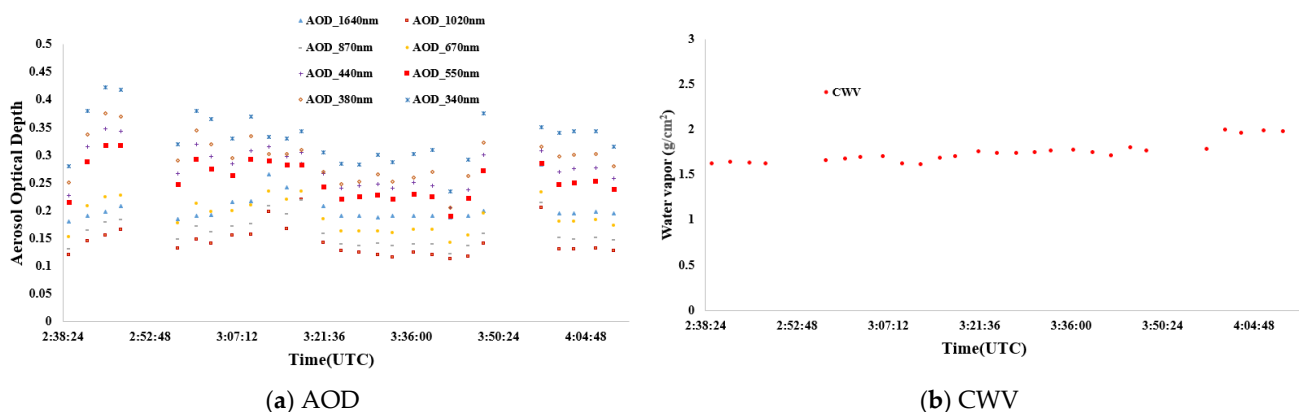


Figure 5. Synchronous measurements of atmospheric parameters at Baotou site on 28 June 2018.

2.5. Measurement of Diffuse-to-Global Irradiance Ratio

In this irradiance-based calibration campaign, the diffuse-to-global ratio at the ground level was the most important parameter, which was measured by an AG-512 SSIR Solar Spectroradiometer. The Chinese Academy of Sciences' Anhui Institute of Optics and Fine Mechanics created the AG-512 SSIR Solar Spectro radiometer. It covered the spectral range from 390 nm to 1030 nm with a spectral resolution of 5 nm. Figure 6 shows AG-512 SSIR Solar Spectroradiometer. When the Solar Spectroradiometer was measuring the diffuse irradiance L_{diff} , the shading board would block the direct beam from solar automatically. The Solar Spectroradiometer would measure the global irradiance L_{global_1} and L_{global_2} when the shading board removed.

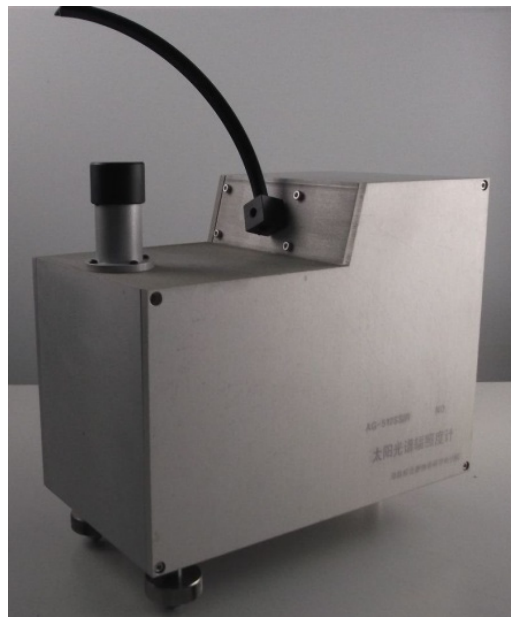


Figure 6. AG-512 SSIR Solar Spectroradiometer.

The diffuse-to-global irradiance ratio (α) is defined as:

$$\alpha = \frac{L_{diff} * 2}{L_{global_1} + L_{global_2}} \quad (10)$$

The diffuse-to-global irradiance ratio was monitored every minute. The synchronized diffuse-to-global irradiance ratio measurements took almost two hours, from about 2:30 to 4:30 (UTM). Figure 7 shows the diffuse-to-total ratio measured by AG-512 SSIR.

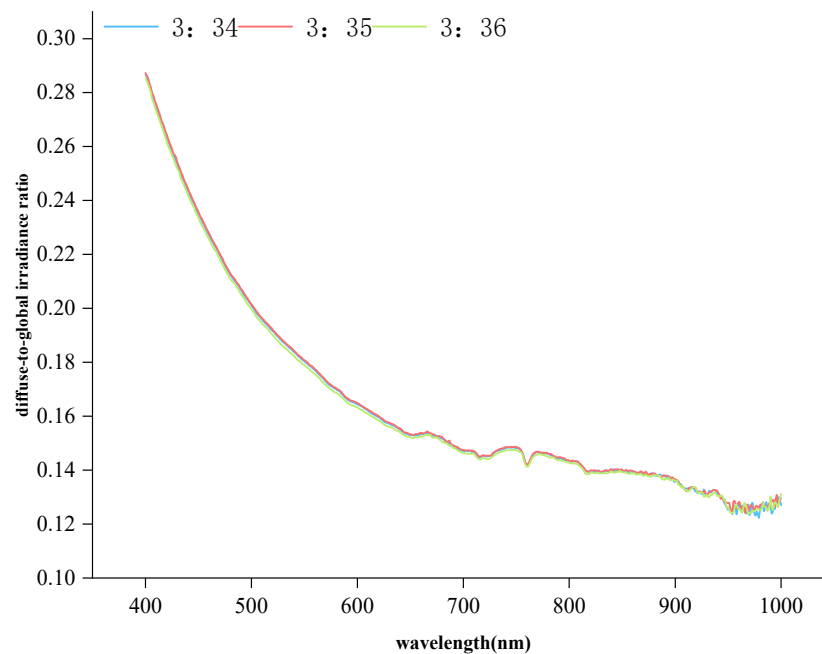


Figure 7. The measured spectrum of the diffuse-to-total ratio measured by AG-512 SSIR.

Using measured diffuse-to-global irradiance ratio $\alpha(\lambda)$ and SRF of MUX $R(\lambda)$, the diffuse-to-global irradiance ratio of each MUX band was calculated as shown in Table 4.

$$\alpha_{band} = \frac{\int \alpha(\lambda)R(\lambda)d\lambda}{\int R(\lambda)d\lambda} \quad (11)$$

Table 4. The diffuse-to-global irradiance ratio of each MUX band.

Time (UTM)	Direction	Diffuse-to-Global Irradiance Ratio			
		MUX-B1	MUX-B2	MUX-B3	MUX-B4
03:35, 28 June 2018	At solar zenith angle α_s	0.2069	0.1792	0.1534	0.1419
	At viewing zenith angle α_v	0.1802	0.1569	0.1345	0.1227
03:38, 3 July 2018	At solar zenith angle α_s	0.1625	0.1218	0.0978	0.0946
	At viewing zenith angle α_v	0.1376	0.0997	0.0767	0.0705

3. Radiometric Calibration Results

The ZY03-02 MUX radiometric calibration coefficients were estimated using an irradiance-based approach and the four nominal reflectance tarps. Figures 8 and 9 show the radiometric calibration results at Baotou site on 28 June and 3 July, 2018. Four nominal reflectance tarps were used for radiometric calibration and two color tarps were used for validation. The difference between these two radiometric calibration coefficients is very small, and the linear correlation coefficient between DN and TOA radiances is higher than 0.99 for each band of ZY3-02 MUX. The calibration results of the irradiance-based method are reliable regardless of high aerosol loading.

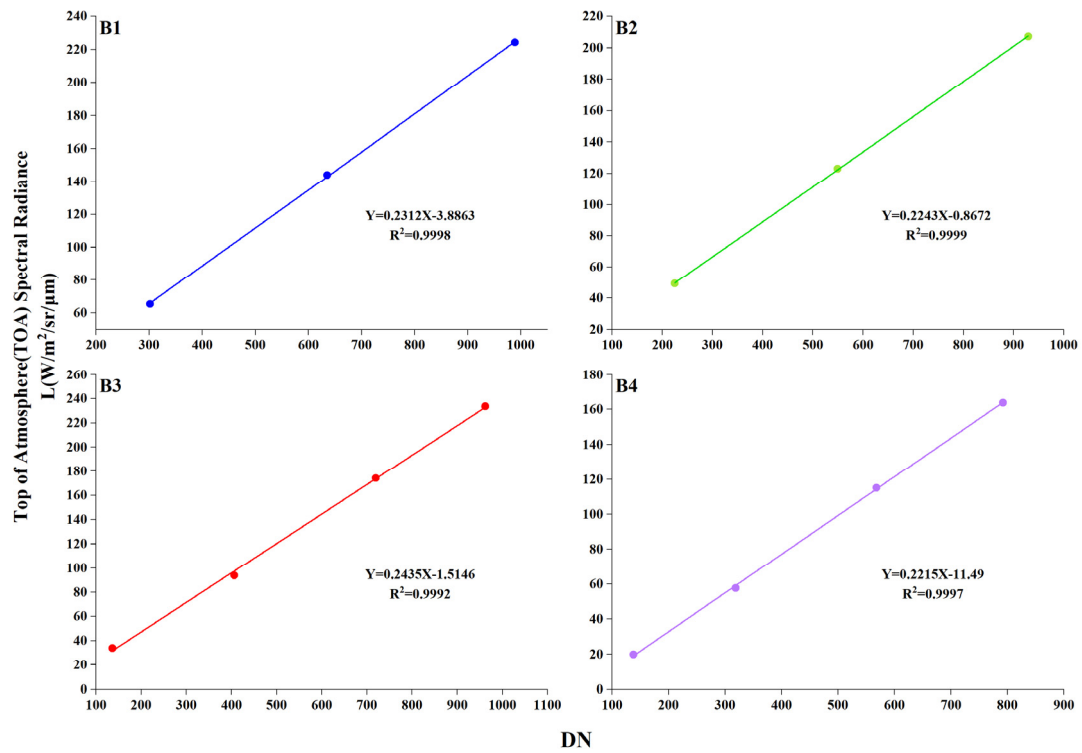


Figure 8. Calibration results using irradiance-based method on 3 July 2018.

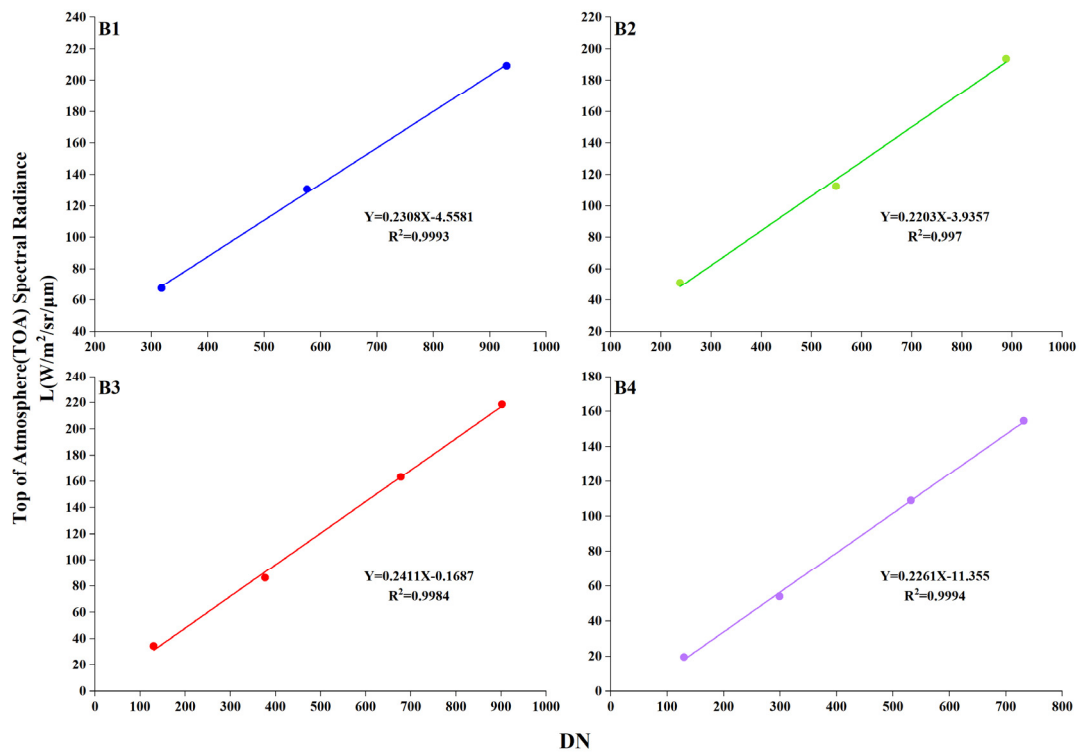


Figure 9. Calibration results using irradiance-based method on 28 June 2018.

The findings of radiometric calibration utilizing the reflectance-based and irradiance-based methods are displayed in Table 5. The findings demonstrated that on 3 July 2018, the reflectance-based and irradiance-based radiometric calibration coefficients were very

consistent. The difference between the two radiometric calibration coefficients of reflectance-based and irradiance-based method were significant on 28 June 2018. Table 5 suggested that coefficients of reflectance-based method on 3 July agreed well with coefficients of irradiance-based method, indicating the error contributed by the assumption of aerosol model parameters with a low aerosol loading (AOD less than 0.1) in the radiative transfer model was very small.

Table 5. Different radiometric calibration coefficients using the reflectance-based and irradiance-based method (in units of $W \times m^{-2} \times sr^{-1} \times \mu m^{-1}$).

Coefficient	Irradiance-Based				Reflectance-Based				Official Coefficient
	3 July 2018		28 June 2018		3 July 2018		28 June 2018		
	Coefficients A		Coefficients B		Coefficients C		Coefficients D		Coefficients E
Band	Gain	Bias	Gain	Bias	Gain	Bias	Gain	Bias	Gain
MUX-B1	0.2312	−3.886	0.2308	−4.558	0.2241	−2.223	0.2102	−6.887	0.2295
MUX-B2	0.2243	−0.867	0.2203	−3.936	0.2192	−0.333	0.2018	−5.039	0.2212
MUX-B3	0.2435	−1.515	0.2411	−0.1687	0.2368	−1.361	0.2176	−1.971	0.2413
MUX-B4	0.2215	−11.49	0.2261	−11.355	0.2186	−11.167	0.2026	−11.478	0.2110

4. Uncertainty Analysis

4.1. Uncertainty Analysis of the Reflectance-Based Method

The reflectance-based uncertainty table listed the major source of radiometric uncertainty of the reflectance-based method (Table 6). Detailed descriptions of the uncertainty were discussed as follows. There are several basic areas of uncertainty in the method: (1) Surface reflectance measurement, (2) Atmospheric characterization, and (3) Inherent accuracy of the MODTRAN 6.0 radiative transfer code.

Table 6. Sources of uncertainties in TOA radiance in the reflectance-based method.

Source of Uncertainty	Accuracy %	TOA Radiance Uncertainty %
Surface reflectance measurement	2.0%	2.0%
Lambertian assumption of targets	2.0%	2.0%
Aerosol optical depth		0.5%
Total columnar water vapor		0.5%
Aerosol type assumption		4.0%
MODTRAN 6.0 Radiative transfer	2.0%	2.0%
Overall Uncertainty		5.68%

The uncertainty in a single measurement of the surface reflectance with SVC HR1024 spectroradiometer is less than 2% [1]. Based on the laboratory calibration tarp BRDF measurements, we can assign a 1.5% error accuracy for assuming a Lambertian calibration tarp [12]. The second primary source of uncertainty in the reflectance-based method is atmospheric characterization, which includes the aerosol optical depth measurement and aerosol type assumption. The AOD and CWV were retrieved by the CE318 software, and a standard rural aerosol type in the MODTRAN 6.0 radiative transfer code was used in this study. The two parameters of aerosol (AOD and aerosol type assumption) resulted in uncertainties of TOA radiance less than 2.0% for AOD and about 4% for aerosol type assumption, respectively. The inherent accuracy of the MODTRAN 6.0 radiative transfer code is less than 1%.

All of the analyzed uncertainty sources above were assumed independent, and the overall uncertainty in the TOA radiance in this reflectance-based approach is 5.68%, less than 6%, as shown in Table 6.

4.2. Uncertainty Analysis of the Irradiance-Based Method

The irradiance-based uncertainty table listed the major source of radiometric uncertainty of the reflectance-based approach (Table 7). Detailed descriptions of the uncertainty were discussed as follows. There are several basic areas of uncertainty in the method: (1) Surface reflectance measurement, (2) Atmospheric characterization, and (3) Inherent accuracy of the MODTRAN 6.0 radiative transfer code.

Table 7. Sources of uncertainties in TOA radiance in the irradiance-based method.

Source of Uncertainty	Accuracy %	TOA Radiance Uncertainty %
Surface reflectance measurement	2.0%	2.0%
Lambertian assumption of targets	2.0%	2.0%
Total columnar water vapor		0.5%
Aerosol optical depth		0.5%
The diffuse-to-global irradiance ratio		2.0%
MODTRAN 6.0 Radiative transfer	2.0%	2.0%
Overall Uncertainty		4.06%

The uncertainty in this method of the surface reflectance is less than 2%, and the 1.5% error accuracy for assuming a Lambertian calibration tarp, as is the same as the reflectance-based method. The AOD resulted in uncertainties of TOA radiance less than 2.0%. The aerosol type with the diffuse-to-global irradiance ratio resulted in uncertainties of TOA radiance less than 1.0%. The inherent accuracy of the MODTRAN 6.0 radiative transfer code is <1%. All of the analyzed uncertainty sources above were assumed independent, and the overall uncertainty in the TOA radiance in this irradiance-based method is 4.06%, less than 5%, as shown in Table 7.

5. Comparison of TOA Radiance Predicted by Reflectance-Based and Irradiance-Based Method

To validate the reliability of the calibration coefficients by irradiance-based method, the TOA radiance of ZY3-02 MUX predicted by reflectance-based and irradiance-based methods using radiative transfer model MODTRAN6.0 (MODerate resolution atmospheric TRANsmiission) was compared with the calculated TOA radiance using DN with the official calibration coefficient of ZY3-02 MUX. Tables 8 and 9 show the difference between the TOA radiance of six calibration tarps predicted by these two calibration methods and the calculated TOA radiance using official calibration coefficient. Difference 1 is the difference between the TOA radiance predicted by irradiance-based method and the calculated TOA radiance using official calibration coefficient. Difference 2 is the difference between the TOA radiance predicted by reflectance-based method and the calculated TOA radiance using official calibration coefficient. As is shown in Tables 8 and 9, all the difference 1 on two separated calibration days were less than 5%, and most difference 2 values were less than 7% on 3 July 2018, but practically all the difference 2 values were more than 7%, and the highest was over 17.51%.

Table 8. Difference between the TOA radiance predicted by calibration methods and the calculated TOA radiance using official calibration coefficient (3 July 2018).

Target	Radiance ($W \times m^{-2} \times sr^{-1} \times \mu m^{-1}$)	MUX-B1	MUX-B3	MUX-B3	MUX-B 4
5% tarp	Calculated TOA	65.822	50.012	35.426	20.012
	Irradiance-based	65.341	49.206	34.852	19.895
	Difference 1	−0.73%	−1.61%	−1.62%	−0.58%
	Reflectance-based	64.526	48.505	33.342	19.61
	Difference 2	−1.97%	−3.01%	−5.88%	−2.01%
20% tarp	Calculated TOA	146.098	127.626	98.755	58.264
	Irradiance-based	144.081	123.031	93.861	57.684
	Difference 1	−1.38%	−3.60%	−4.96%	−1.00%
	Reflectance-based	141.854	120.828	90.681	55.531
	Difference 2	−2.90%	−5.33%	−8.18%	−4.69%
40% tarp	Calculated TOA	229.874	214.558	177.232	117.828
	Irradiance-based	224.211	207.192	174.124	115.071
	Difference 1	−2.46%	−3.43%	−1.75%	−2.34%
	Reflectance-based	218.521	201.485	168.319	110.08
	Difference 2	−4.94%	−6.09%	−5.03%	−6.58%
Red tarp	Calculated TOA	91.283	72.367	131.224	94.394
	Irradiance-based	90.049	70.925	127.276	90.788
	Difference 1	−1.35%	−1.99%	−3.01%	−3.82%
	Reflectance-based	87.426	68.377	123.261	88.734
	Difference 2	−4.23%	−5.51%	−6.07%	−6.00%
Blue tarp	Calculated TOA	223.765	133.622	97.872	145.121
	Irradiance-based	218.969	129.619	94.397	143.698
	Difference 1	−2.14%	−3.00%	−3.55%	−0.98%
	Reflectance-based	216.247	126.458	92.22	138.771
	Difference 2	−3.36%	−5.36%	−5.77%	−4.38%

Table 9. Difference between the TOA radiance predicted by calibration methods and the calculated TOA radiance using official calibration coefficient (28 June 2018).

Target	Radiance ($W \times m^{-2} \times sr^{-1} \times \mu m^{-1}$)	MUX-B1	MUX-B3	MUX-B3	MUX-B 4
5% tarp	Calculated TOA	68.726	51.306	36.013	20.023
	Irradiance-based	67.59	50.85	34.225	19.489
	Difference 1	−1.65%	−0.89%	−4.96%	−2.67%
	Reflectance-based	61.836	46.904	30.281	16.517
	Difference 2	−10.03%	−8.58%	−15.92%	−17.51%
20% tarp	Calculated TOA	134.76	115.368	88.776	56.212
	Irradiance-based	130.538	112.446	86.215	54.141
	Difference 1	−3.13%	−2.53%	−2.88%	−3.68%
	Reflectance-based	123.162	105.054	81.214	50.573
	Difference 2	−8.61%	−8.94%	−8.52%	−10.03%
40% tarp	Calculated TOA	214.568	196.655	167.322	111.497
	Irradiance-based	209.178	193.818	163.4	109.059
	Difference 1	−2.51%	−1.44%	−2.34%	−2.19%
	Reflectance-based	197.551	182.289	155.642	103.456
	Difference 2	−7.93%	−7.31%	−6.98%	−7.21%

Table 9. Cont.

Target	Radiance ($W \times m^{-2} \times sr^{-1} \times \mu m^{-1}$)	MUX-B1	MUX-B3	MUX-B3	MUX-B 4
Red tarp	Calculated TOA	86.965	67.396	116.577	84.146
	Irradiance-based	84.997	64.606	113.47	80.395
	Difference 1	−2.26%	−4.14%	−2.67%	−4.46%
	Reflectance-based	77.812	59.349	105.871	75.345
	Difference 2	−10.52%	−11.94%	−9.18%	−10.46%
Blue tarp	Calculated TOA	213.335	128.672	89.423	133.984
	Irradiance-based	205.622	122.945	85.249	128.179
	Difference 1	−3.62%	−4.45%	−4.67%	−4.33%
	Reflectance-based	191.101	114.291	78.266	120.191
	Difference 2	−10.42%	−11.18%	−12.48%	−10.29%

The assumption of the aerosol model in the radiative transfer model with a high AOD brings errors in the prediction of the TOA radiance, so the difference between these two TOA radiances using different methods was relatively high. This comparison also suggested that the irradiance-based predicted TOA radiance using the radiative transfer model was reliable and stable, no matter high or low aerosol loading. The irradiance-based absolute radiometric calibration method demonstrated obvious improvement with the reflectance-based method.

6. Conclusions

An improved calibration campaign using the irradiance-based absolute radiometric calibration method between June and July 2018 at Baotou calibration site was presented in this study. The linear relationship between DNs of satellite sensor and TOA radiances at each MUX band was established to obtain a stable and reliable absolute calibration coefficient for MUX sensor.

The reflectance-based absolute radiometric calibration campaign was performed for ZY3-02 MUX more than twice a year since July 2016 [12]. The calibration reflectance-based should be updated when a new DN-to-radiance coefficient was determined in each calibration campaign. In this study, two reflectance-based coefficients were obtained by the two separate campaigns, and a discrepancy between these two coefficients was significant. This study suggested that the reflectance-based radiometric calibration method is acceptable when the aerosol loading in the atmosphere is relatively low (AOD is less than 0.1). If the AOD is more than 0.25, the errors from the assumption of the aerosol model in the radiative transfer model is too large, thus affecting the reliability and stability of radiometric calibration results. The irradiance-based absolute radiometric calibration coefficients, on the other hand, were both consistent and reliable in both separate campaigns, and showed good consistency between the irradiance-based predicted TOA radiances using MODTRAN 6.0, regardless of high or low aerosol loading. In this study, distinct advantages of this irradiance-based method were demonstrated for monitoring the radiometric characteristics of ZY3-02 MUX. In future work, LASAC plans to conduct the radiometric calibration campaign several times a year using irradiance-based method to obtain high-accuracy and reliable calibration results.

Author Contributions: H.T. developed the research plan and supervised the work, J.X., H.W., H.Z. and W.C. participated in the literature review, method selection, data acquisition, and discussions. All authors have read and agreed to the published version of the manuscript.

Funding: This work was supported by the National Key R&D Program of China, 2022YFB3903000, 2022YFB3903005, 2022YFB3903200, 2022YFB3903201.

Institutional Review Board Statement: Not applicable.

Informed Consent Statement: Not applicable.

Data Availability Statement: Not applicable.

Conflicts of Interest: The authors declare no conflict of interest.

References

1. Thome, K.J. Absolute Radiometric Calibration of Landsat 7 ETM+ Using the Reflectance-Based Method. *Remote Sens. Environ.* **2001**, *78*, 27–38. [[CrossRef](#)]
2. Dinguirard, M.; Slater, P.N. Calibration of Space-Multispectral Imaging Sensors: A Review. *Remote Sens. Environ.* **1999**, *68*, 194–205. [[CrossRef](#)]
3. Biggar, S.F.; Dinguirard, M.C.; Gellman, G.I.; Henry, P.; Jackson, R.D.; Moran, M.S.; Slater, P.N. Radiometric Calibration of SPOT 2 HRV-a Comparison of Three Methods. *Proc. SPIE* **1991**, *1493*, 155–162.
4. Gao, H.L.; Gu, X.F.; Yu, T. The Research Overview on Visible and Near-infrared Channels Radiometric Calibration of Space-borne Optical Remote Sensors. *Remote Sens. Inf.* **2010**, *4*, 12.
5. Frouin, R.; Gautier, C. Calibration of NOAA-7 AVHRR, GOES-5, and GOES-6 VISSR/VAS solar channels. *Remote Sens. Environ.* **1987**, *22*, 73–101. [[CrossRef](#)]
6. Pagnutti, M.; Ryan, R.E.; Kelly, M.; Holekamp, K.; Zannoni, V.; Thome, K.; Schiller, S. Radiometric characterization of IKONOS multispectral imagery. *Remote Sens. Environ.* **2003**, *88*, 53–68. [[CrossRef](#)]
7. Xiong, X.; Barnes, W.; Xie, X.; Salomonson, V. On-orbit performance of Aqua MODIS on-board calibrators. *Proc. SPIE* **2005**, *5978*, 75–80.
8. Ponzoni, F.J.; Junior, J.Z.; Lamparelli, R. In-flight absolute calibration of the CBERS-2 CCD sensor data. *An. Acad. Bras. Ciênc.* **2008**, *80*, 799–804. [[CrossRef](#)] [[PubMed](#)]
9. Hu, X.; Liu, J.; Sun, L.; Rong, Z.; Li, Y.; Zhang, Y.; Zheng, Z.; Wu, R.; Zhang, L.; Gu, X. Characterization of CRCS Dunhuang test site and vicarious calibration utilization for Fengyun (FY) series sensors. *Can. J. Remote Sens.* **2010**, *36*, 566–582. [[CrossRef](#)]
10. Naughton, D.; Brunn, A.; Czapla-Myers, J.; Douglass, S.; Thiele, M.; Weichert, H.; Oxford, M. Absolute radiometric calibration of the RapidEye multispectral imager using the reflectance-based vicarious calibration method. *J. Appl. Remote Sens.* **2011**, *5*, 3544. [[CrossRef](#)]
11. Tang, H.; Xie, J.; Tang, X.; Chen, W.; Li, Q. On-Orbit Radiometric Performance of GF-7 Satellite Multispectral Imagery. *Remote Sens.* **2022**, *14*, 886. [[CrossRef](#)]
12. Tang, H.; Xie, J.; Tang, X.; Chen, W.; Li, Q. On-Orbit Absolute Radiometric Calibration and Validation of ZY3-02 Satellite Multispectral Sensor. *Sensors* **2022**, *22*, 2066. [[CrossRef](#)] [[PubMed](#)]
13. Bouvet, M.; Thome, K.; Berthelot, B.; Bialek, A.; Czapla-Myers, J.; Fox, N.P.; Goryl, P.; Henry, P.; Ma, L.; Marcq, S.; et al. RadCalNet: A Radiometric Calibration Network for Earth Observing Imagers Operating in the Visible to Shortwave Infrared Spectral Range. *Remote Sens.* **2019**, *11*, 2401. [[CrossRef](#)]
14. Li, C.R.; Ma, L.L.; Tang, L.L.; Gao, C.X.; Qian, Y.G.; Wang, N.; Wang, X.H. A comprehensive calibration site for high resolution remote sensors dedicated to quantitative remote sensing and its applications. *Natl. Remote Sens. Bull.* **2021**, *25*, 198–219.
15. Yeom, J.-M.; Hwang, J.; Jung, J.-H.; Lee, K.-H.; Lee, C.-S. Initial Radiometric Characteristics of KOMPSAT-3A Multispectral Imagery Using the 6S Radiative Transfer Model, Well-Known Radiometric Tarps, and MFRSR Measurements. *Remote Sens.* **2017**, *9*, 130. [[CrossRef](#)]

Disclaimer/Publisher’s Note: The statements, opinions and data contained in all publications are solely those of the individual author(s) and contributor(s) and not of MDPI and/or the editor(s). MDPI and/or the editor(s) disclaim responsibility for any injury to people or property resulting from any ideas, methods, instructions or products referred to in the content.